Journal of Neuroscience Methods 362 (2021) 109319

Contents lists available at ScienceDirect

Journal of Neuroscience Methods

journal homepage: www.elsevier.com/locate/jneumeth

A versatile system for neuromuscular stimulation and recording in the mouse model using a lightweight magnetically coupled headmount

Annie Vahedipour [a,*], Matthew R. Short [b], Azadeh Timnak [c], Omid Haji Maghsoudi [d], Thomas Hallowell [e], Jonathan Gerstenhaber [f], Ornella Cappellari [g], Michel Lemay [f], Andrew J. Spence [f]

[a] Department of Pediatrics, Neurology, Yale University, New Haven, CT 06510, USA
[b] Functional and Applied Biomechanics Section, Rehabilitation Medicine Department, National Institutes of Health, Bethesda, MD 20814, USA
[c] Laboratory for Cell and Medicine, School of Medicine, Stanford University, Palo Alto, CA 94304, USA
[d] Department of Radiology, University of Pennsylvania, Philadelphia, PA 19104, USA
[e] Anesthesiology and Critical Care Medicine, Children's Hospital of Philadelphia, Philadelphia, PA 19104, USA
[f] Department of Bioengineering, Temple University, Philadelphia, PA 19122, USA
[g] Department of Pharmacy-Drug Science, University of Bari "Aldo Moro", 70125 Bari, Italy

ARTICLE INFO

Keywords:
Rodents
Headmount
Headstage
Muscle stimulation
Nerve stimulation
Optogenetics

ABSTRACT

Neural stimulation and recording in rodents are common methods to better understand the nervous system and improve the quality of life of individuals who are suffering from neurological disorders (e.g., epilepsy), as well as for permanent reduction of chronic pain in patients with neuropathic pain and spinal-cord injury. This method requires a neural interface (e.g., a headmount) to couple the implanted neural device with instrumentation system. The size and the total weight of such headmounts should be designed in a way to minimize its effect on the movement of the animal. This is a crucial factor in gait, kinematic, and behavioral neuroscience studies of freely moving mice. Here we introduce a lightweight 'snap-in' electro-magnetic headmount that is extremely small, and uses strong neodymium magnetics to enable a reliable connection without sacrificing the lightweight of the device. Additionally, the headmount requires minimal surgical intervention during the implantation, resulting in minimal tissue damage. The device has demonstrated itself to be robust, and successfully provided direct electrical stimulation of nerve and electrical muscle stimulation and recording, as well as powering implanted LEDs for optogenetic use scenarios.

1. Introduction

Optical and electrical neural stimulation and recording are critical tools in experiments with freely-behaving rodents. This is especially true for mice, as they are becoming increasingly popular in locomotor studies (Talpalar and Kiehn, 2010; Bellardita and Kiehn, 2015; Harris-Warrick, 2011; Akay et al., 2014). This growing interest is largely due to the available set of disease models and genetic tools, which enable precise manipulation of many neurophysiological aspects of these subjects (Arenkiel et al., 2007; Costa et al., 2002; Lathe, 1996).

Neuromuscular electrical stimulation and electrophysiological recording support many options in the treatment of muscle and nerve injuries, such as in spinal cord injury (Kadekaro et al., 1985; Moreno-Duarte et al., 2014; Dobkin et al., 1995) or active prosthetic limbs (Wang et al., 2013; Ortiz-Catalan et al., 2014). Additionally, optogenetic studies in freely running mice have sought to understand multiple neurological concerns including spinal cord injury (Caggiano et al., 2014) and Parkinson's disease (Kravitz et al., 2010). Optogenetics is a neural manipulation technique that allows for activation or inhibition of specific neurons using illumination with light (Deisseroth, 2011). Light must be delivered to these neurons, however, and it has a short (typically ~150 μm) penetration depth, making delivery of light with LEDs placed around nerves an important approach (Song et al., 2018; Llewelyn et al., 2010).

Both neuromuscular stimulation and recording in freely moving mice require interfaces (i.e., headmounts) to couple the implanted neural device with the optical/electrophysiological hardware. The challenge of building such headmounts is exacerbated at rodent scale (e.g., mice)

* Correspondence to: Department of Pediatrics, Neurology, Yale University School of Medicine, 15 York St., New Haven, CT 06510, USA .
E-mail address: annie.vahedipour@yale.edu (A. Vahedipour).

https://doi.org/10.1016/j.jneumeth.2021.109319
Received 6 November 2020; Received in revised form 6 August 2021; Accepted 9 August 2021
Available online 13 August 2021

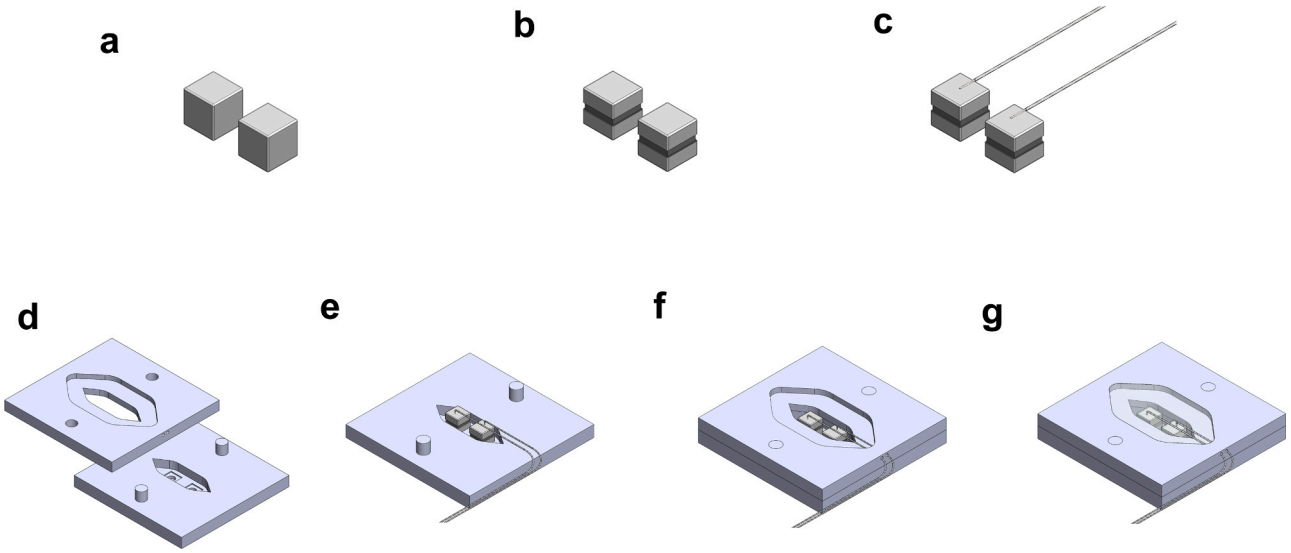

Fig. 1. Fabrication of the headmount from PDMS using a mold. (a) Two neodymium magnets. (b) The magnets were ground down in order to increase pull-out force from the headmount. (c) Stainless steel wires soldered to the magnets. (d) 3D-printed mold. (e, and f) Magnets and wires positioned within the mold. (g) The mold filled with PDMS that create the headmount.

compared to primates with larger and more ready affixed transcutaneous connectors or electrode arrays themselves. Several factors need to be considered when designing headmounts compatible with mice.

The size and total weight of the apparatus should be designed in a way that minimizes the effect of the attached headmount on the movement of the animal. This is a crucial factor in gait, kinematic, and behavioral neuroscience studies of freely moving mice, where the normal weight range for an adult mouse is only 18–35 g (Dutta and Sengupta, 2016). There are various headmounts available for studies of central nervous system, however they are usually large in size and not readily adaptable for interfacing with the peripheral nervous system (Zhang et al., 2019; Jeong et al., 2015; Kitanishi et al., 2021). Wireless headmounts, on the other hand, require either a wireless power supply or a complex supplemental system to function (Zhang et al., 2019; Jeong et al., 2015; Montgomery et al., 2015). In most wireless use cases, a miniature wireless driver is used. The smaller ones, which are still typically more massive and voluminous than wired headmounts and are designed for more free movement of the mouse, normally have a battery life limitation. For longer experimental times, a high capacity battery is needed, but this comes at the expense of significantly more mass (~1.3 g) (Hashimoto et al., 2014). Montgomery et al. introduced a miniature wireless headmount for peripheral studies that did not require attachment of the heavy LED drivers to the headmount itself, but the experiments could only be conducted inside a specific chamber that supplies the power, which limits the number and type of experiments that can be carried out (Montgomery et al., 2015). A more recent study by Lee et al. (2018a) introduced a small peripheral nerve recording and stimulation system with headmount connector for experiments on freely moving animals, but this is still $3 \times 1.5 \times 0.5$ cm^3 in size and weighs 2.8 g (Lee et al., 2018b).

It is also important to minimize the surgical intervention and avoid skull trepanation (creating a hole in the skull that exposes the dura mater) during the implantation. Screws and dental acrylic are the most common method of implanting headmounts. Although this method works well for adult animals (Riban et al., 2002; Park et al., 2019), it may be more problematic when utilized in young mice or other animal models. The limitation of the screw-based technique is due to the fact that young mice skulls are not strong enough to hold the anchoring screws (Wu et al., 2009). Using anchoring screws also enhances the chance of traumatic injury or death from infection, stroke, epilepsy, or brain abscesses. The afore-mentioned surgical complications can be a major concern in studying disease models, due to the vulnerability of these animals to the intracranial surgery.

Furthermore, it is favorable for the designed headmount to maintain its position securely after implantation for long-term neurophysiological studies in mice. In this study, a novel interfacing method using cyanoacrylate glue is developed. While Marrosu et al. (2006) and Wu et al. (2008) have successfully used epoxy and glue to hold electrodes on the skull of the mice, it remains to be established whether using cyanoacrylate glue is adequate to secure the headmount to the dermis of the skin. Additionally, commonly used headmounts are frequently hard to connect and disconnect, because they rely on pin connectors that require relatively high insertion force, that can harm the animal or the animal handler (Park et al., 2019). This is especially relevant for mice that have thinner and more fragile skull bones.

Here we introduce a lightweight 'snap-in' electro-magnetic headmount that results in near zero insertion force and causes less stress on animal and researcher. Methods are further described for coupling the headmount to an electrical and an optical nerve cuff, and to muscle directly for muscle stimulation and electromyographic (EMG) measurements.

2. Materials and methods

The system consists of the magnetic headmount anchored to the animal, coupled internally to an implantable neural device, and a mating magnetic connector for external coupling to the headmount and connection to the external instrumentation.

2.1. Headmount fabrication

Two neodymium magnets (Apex Magnets, PN M12CU), shown in Fig. 1a, were used for each headmount. Such magnets are small and light, while maintaining a pull force of up to 1lb, which is low enough to be pulled off without injury to animal, but high enough that they remain well connected during a vigorous exercise. We modified the magnets to increase pull-out force from the headmount. To do this, we ground a thin groove around the perimeter (Fig. 1b) to create a rough surface. This results in a better bond between the magnets and the PDMS around them that will be added later. Stainless steel wires were soldered to the magnets (Fig. 1c). To do this, we striped off ~4 mm of the Teflon from

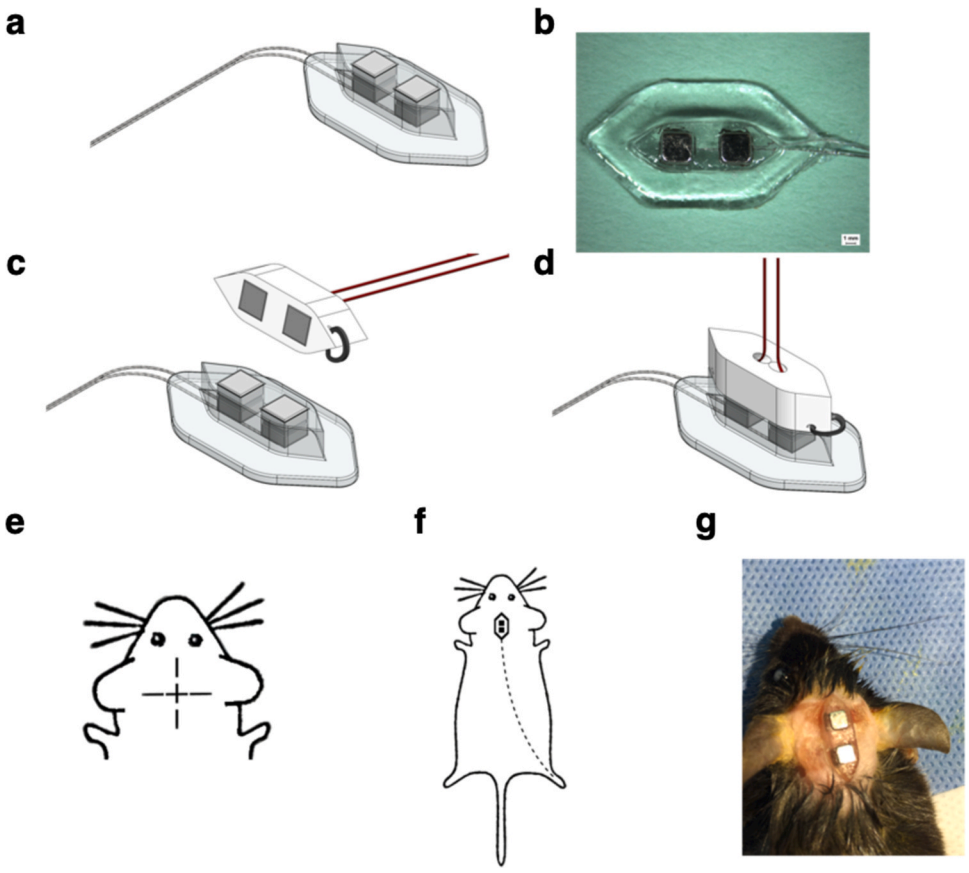

Fig. 2. The completed headmount. (a) Solidworks drawing, and (b) the actual device. The lightweight headmount is extremely small, and uses strong permanent magnets for self-alignment, enabling a reliable connection without a large mass. A magnetically mating coupler carries two conductors off the headmount and to external instrumentation. (c) shows before the connection and, (d) shows after. A small loop of silk suture is also embedded in the coupler to facilitate removal of the coupler with force primarily in shear, thus reducing the direct pressure on the animals' head. For the headmount implantation surgery, two incision are first made for implanting the headmount on top of the skull (e), and wires are tunneled from the headmount to the target nerve or limb (f). (g) is the Photograph of the implanted headmount.

the end of the wire using a #10 scalpel blade. A small amount of a liquid flux (Harris, PN SBSKPOP) was applied to the de-insulated strands of the wire and one of the square faces of the magnet. We then brought the temperature of the soldering iron to 400 °C and use it to melt the solder on the de-insulated wire. Using the soldering iron, the tinned wire was connected to the magnet. We applied adhesive over the solder joints using optical adhesive and UV curing gun to provide stress relief and insulation (Norland Optical Adhesive 81; ThorLabs UV Curing System, PN CS2010). We designed and 3D-printed a mold to reproducibly fabricate the headmount (Fig. 1d). Magnets and wires were positioned within the mold to be filled with PDMS, that create the headmount (Fig. 1e). They were positioned with opposite poles present on the top of the headmount, enabling the connection to be self-aligning. A headmount coupler, described in 2.2, was used on the other side of the mold to hold the magnets in place and keep them from snapping together, and was not removed until after the PDMS around the magnets was cured. The wires were embedded and exited from the PDMS membrane (Fig. 1f and g). In this manner the wires did not have to be manually orientated during surgery. Furthermore, this reduce the risk of the wires being exposed during significant activity.

The headmount design has two main components: (1) a small rectangular prism with magnets mounted flush with the top surface, that is visible outside the skin; (2) a larger, thin, flat membrane that sits under the skin and above the bone to hold the mount in place (Fig. 2a and b). The headmount is very lightweight and small in size. Its dimensions are 1.2 cm × 4 mm and it weighs 0.4 g, which aids in animal stability, and affords coupling to the skin and bone of the animal with cyanoacrylate adhesive.

2.2. Instrument coupler fabrication

We used a 3D-printed coupler shown in Fig. 2c and d to connect the headmount to the external instrument. The coupler holds two magnets of opposing polarities, which have wires connected as in the headmount, but the wires are allowed to leave at an angle. The coupler also includes a pull-string allowing easy removal at an angle. Together this means that during removal there is reduced stress on the wires, and the force on the headmount is mostly in shear, reducing the pressure felt by the animal.

2.3. Headmount Implantation

We fabricated headmounts and implanted them on the heads of adult female C57BL/6J mice (http://jaxmice.jax.org/strain/013636.html). Animals were housed under a 12:12 h light-dark cycle in a temperature-controlled environment with food and water available ad libitum. All animal procedures were approved by the Temple University Institutional Animal Care and Use Committee (IACUC) under protocols #4319 and #4675 (AJS) (Vahedipour et al., 2018). All procedures in mice were carried out in accordance with the relevant guidelines and regulations of the Temple University IACUC, under the Animal Care and Use Protocol (ACUP) #4675.

To implant the headmount, we make a perpendicular incision on top of the head of the animal as shown in Fig. 2e. In the example shown in Fig. 2f and g, we are connecting the two wires to the mouse lateral gastrocnemius muscle, for direct muscle stimulation and recording. We therefore make a further incision in the leg above this target muscle (a similar incision is made for nerve cuff applications). We first ran a thin metal rod with a Teflon tubing around it that holds the wires under the skin to clear a tunneled path under the skin from the head incision to the target site. This reduces the local tissue damage (Fig. 2f). After the wires are pulled through the tunnel, the tube is removed. In case of implanting nerve cuff, the cuff is also passed through the tubing. The metal rod was used in some cases to push the cuff gently through the tubing. The dorsal surface of the PDMS membrane of the headmount (that points towards

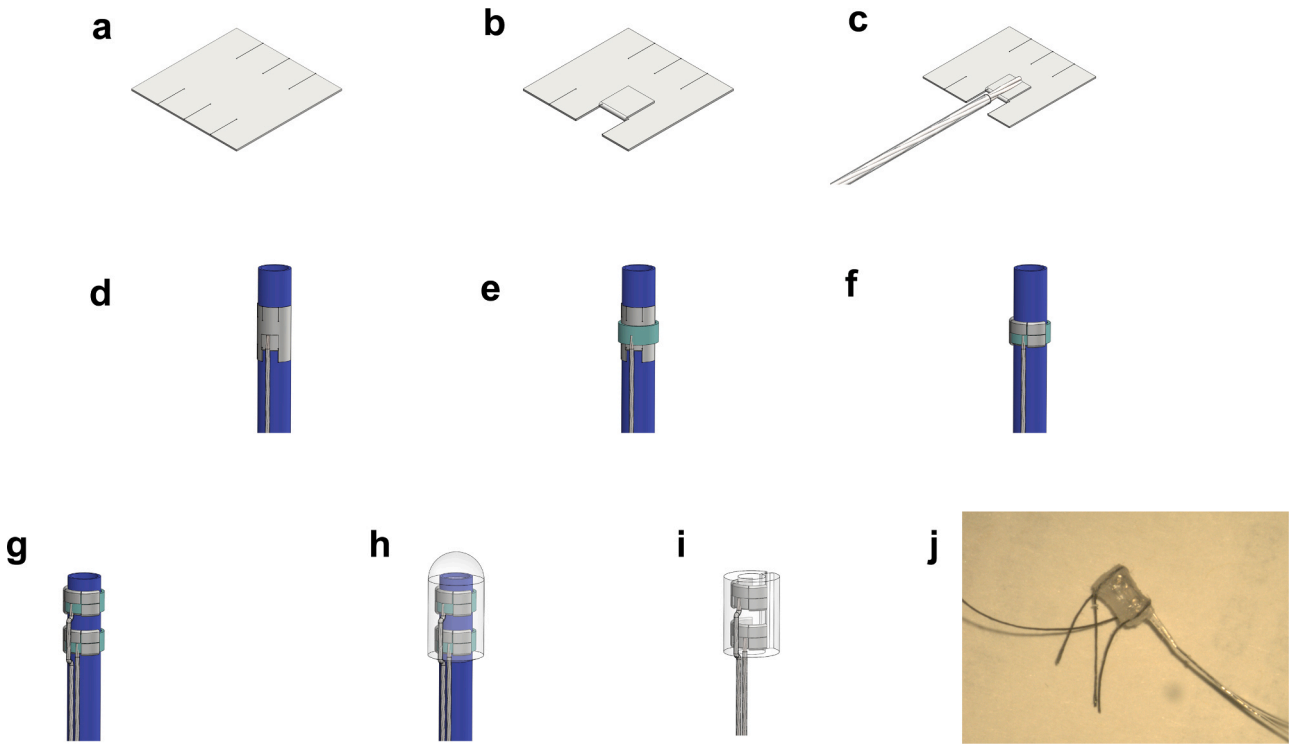

Fig. 3. Electrical neural cuff fabrication. (a) Two (2 mm × 2 mm) Platinum plates were used for the two electrodes, and four equally spaced flaps were created on each side of the plates. (b) The plate with a flipped flap. (c) The plate soldered to a 40 AWG Teflon coated-stainless steel wire (Cooner Wires AS 631). (d) The plate wrapped around a mandrel that was used as the nerve mold. (e) Silastic band wrapped around and secured the plate on the mandrel. (f) Flaps of the plates flipped around the silastic band. (g) The second electrode positioned on the mandrel at a 2 mm distance from the first electrode. (h) The mandrel coated with diluted medical adhesive. (i) The completed electrical nerve cuff. (j) Sutures integrated to enhance long-term viability of the module.

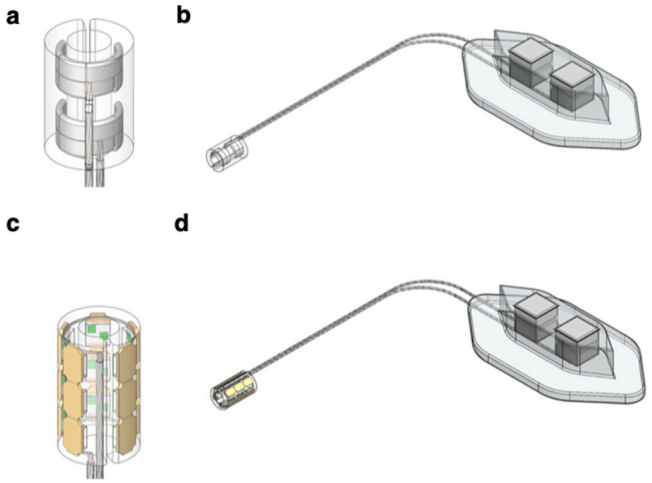

Fig. 4. Coupling the headmount to different types of neural cuffs. (a) Detail of bipolar neural cuff, and (b) coupled to the headmount. We tested the headmount for nerve stimulation scenarios by coupling it to an electrical nerve cuff and implanting the device around the sciatic nerve and on the head of the mouse. (c) Optical nerve cuff, and (d) coupled to the headmount. Additionally, we tested the headmount for optical nerve stimulation scenarios by connecting it to an optical nerve cuff.

the underside of the skin) is coated with a small amount of cyanoacrylate glue which then bonds to the dermis of the skin. Thus, the headmount is implanted on top of the skull of the mouse (Fig. 2g).

2.4. Validation of the headmount in three use cases

We used the headmount to provide direct electrical stimulation of nerve and electrical muscle stimulation and recording, as well as to power implanted LEDs for optogenetic use scenarios.

2.4.1. Electrical nerve stimulation

A bipolar implantable cuff electrode for electrical stimulation of small diameter peripheral nerves of rodents was fabricated as shown in Fig. 3. We used the method introduced by Haugland (1996) to build the electrical cuffs with a slight modification to the design. We note the sizes described here are for use in mouse sciatic nerve, but can be readily modified for other rodents and other nerves. Two (2 mm × 2 mm) Platinum plates were used for the two electrodes as it is highly conductive and non-oxidizing. Four equally spaced flaps were created on each side of the plates by cutting 0.5 mm deep sections with micro-scissors (Fig. 3a; Fine Science Tools 15018-10), out of which one was flipped back to use as a space for the connecting the wire (Fig. 3b). We then soldered 0.28 mm diameter 40 AWG Teflon coated-stainless steel wire (Cooner Wires, PN AS631; Fig. 3c) to the plate. This method proved to be a cleaner and easier way of making this connection, compared to the previously published spot-welding method (Haugland, 1996), but requires the use of specialized soldering techniques and flux. Namely, we used STA-BRITE Silver Solder and Harris Stay-Clean Liquid Soldering Flux and the soldering had to be done at high temperature of 400 °C. The wire is relatively flexible and robust with a small diameter, which reduces the chances of damage and of irritating the animal after implantation. We used Zeus PTFE light wall tubing (0.76 mm O.D.) as a nerve mold (Fig. 3d). The plates were positioned and fixed on the mandrel with a silastic band (0.94 mm O.D.) (Fig. 3e). The flaps of the plates were subsequently flipped around the band (Fig. 3f). The second electrode was constructed similarly and positioned on the mandrel at a 2 mm distance from the first electrode (Fig. 3g). We used diluted

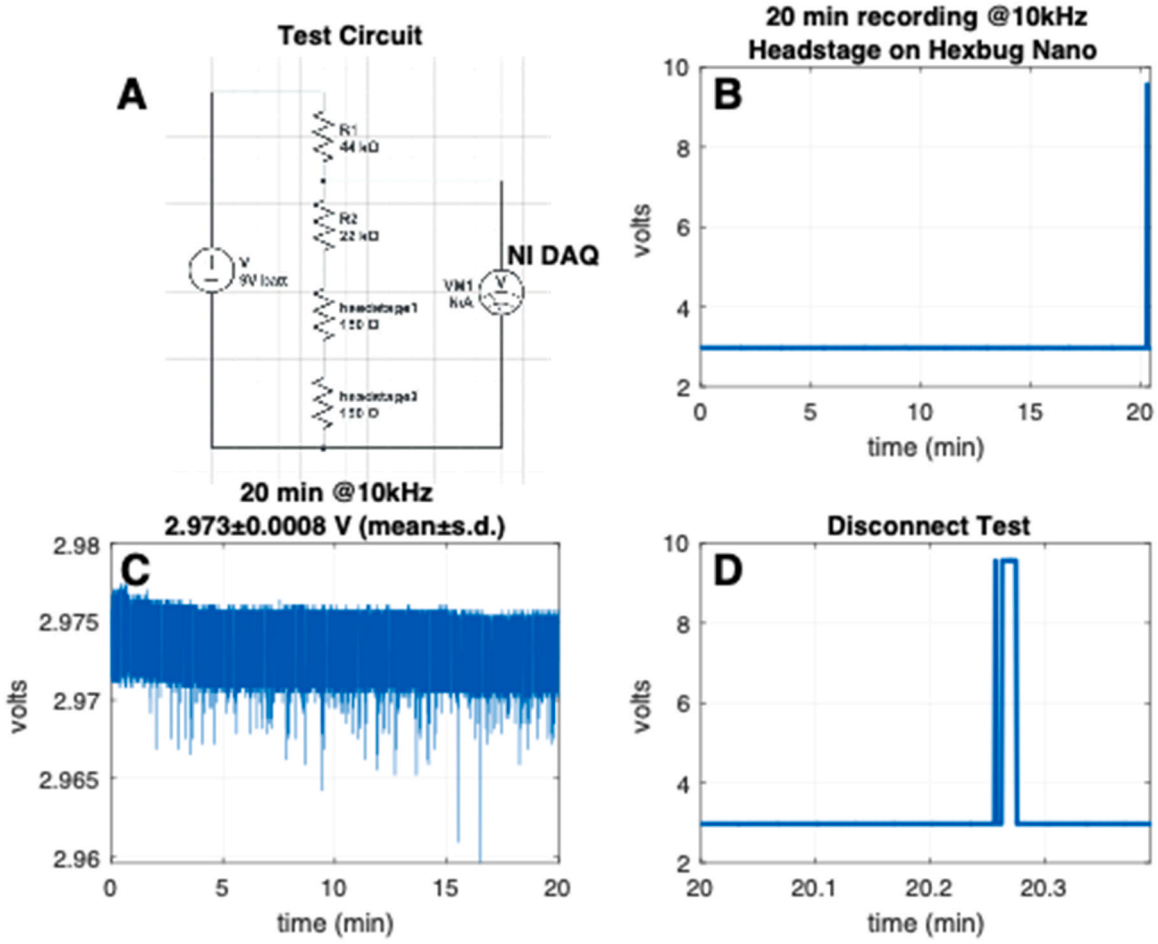

Fig. 5. Continuous measurement of resistance for a shorted headmount attached to a moving HexBug (a) The circuit used to record analog voltage whilst the HexBug was moving. (b) and (c) Voltage recording of the headmount at 10 kHz for 20 min. (d) Voltage recording of the headmount when disconnecting the coupler after 20 min.

medical adhesive (Factor II, PN A100) to coat the assembly and thus embed the electrodes, forming a flexible cuff (Fig. 3h). We applied a second coat 4 h following the first coat. The coated mandrel was later cut into the desired cuff size, after the silicone was cured (24 h left in the room temperature; Fig. 3i). The new design also integrates sutures to enhance long-term viability of the module by preventing dislodgment. This further makes for easier and safer implantation, because the sutures function as handles for the cuff, allowing careful opening and closing around the nerve with less force and operator manipulation (Fig. 3j). The electrical cuff was then coupled with the headmount (Fig. 4a and b).

To test nerve stimulation using our headmount, we implanted a headmount coupled with the cuff electrode around the sciatic nerve of one mouse. Before suturing the incision in anesthetized mouse, electrical current was applied to the nerve by connecting the headmount to the stimulator via its coupler. This stimulates the sciatic nerve and subsequently causes contraction of distal leg muscles and helps with validating the device functionality and the surgery. We connected the animal's foot to a footplate and measured the amount of torque produced by different currents for nerve stimulation using an Aurora muscle lever system (model # A806D). This was done to find the correct range of currents required for an average force production by nerve stimulation. In day five of the surgery, we had the animal run on a treadmill and disturbed its gait by applying the determined range of currents to the nerve of the mouse via its headmount connector. We used an automated camera-treadmill system (Spence et al., 2013; Vahedipour et al., 2018) to monitor the paw positions of the mouse (Maghsoudi et al., 2019) during nerve stimulation.

2.4.2. *Electrical muscle stimulation and electromyography*

We further tested the device with direct muscle stimulation and recording in mice. In this case, we used our headmounts coupled to wires that were de-insulated near the tips and directly tied into the lateral gastrocnemius (LG) muscle of mice. We stimulated the LG muscle using different electrical currents and measured the ankle torsion produced by the muscle stimulation using the same Aurora muscle lever system. We later used this activation of LG muscle to perturb the gait of trotting mice to explore the control and regulation of gait in mice as described in 2.4.1. We further used the headmount to measure the electromyographic EMG activity of the LG muscle in vivo, for running mice.

2.4.3. *Optical nerve stimulation*

Finally, the headmount was coupled to a custom optical LED cuff designed for optogenetic stimulation. The optical cuff was made of 15 Blue Pico-LEDs (Digikey 846-1112-1-ND) soldered together that were embedded in medical adhesive (Fig. 4a and b). The array consisted of 5 linear arrays of 3 LEDs in series; e.g., 6 "strings" or 3 LEDs in series were placed in parallel. We measured the output optical power to validate the current capacity of the tunneled wires.

3. Results

3.1. *Durability and resistivity*

We successfully implanted eight headmounts on the head of eight mice to check for the durability of the device. The animals were

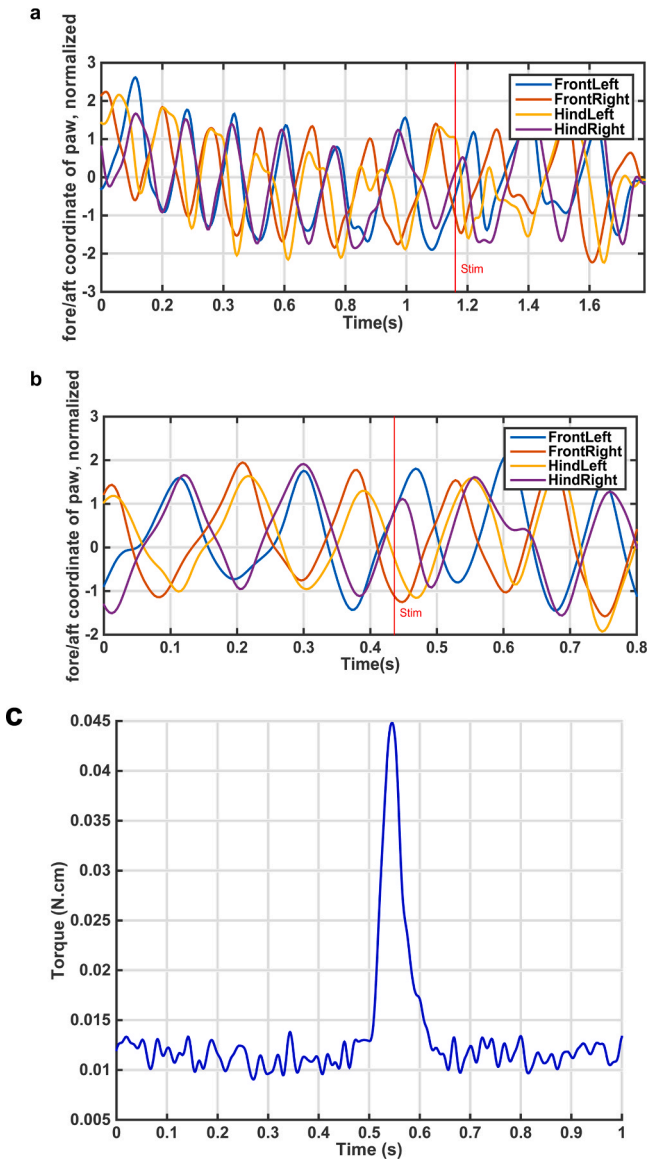

Fig. 6. Validating the headmount for electrical muscle and nerve stimulation, Fore/aft paw positions for ~1 s before, and 0.5 s after electrical stimulation of (a) the sciatic nerve, and (b) the lateral gastrocnemius muscle. Line color denotes paw. Positions are relative to a body centroid computed as the median of all four paw positions, and normalized by z-scoring. The red bar indicates the electrical stimulation trigger time. The stimulated (purple) paw is seen to make an abbreviated swing cycle, making contact with the ground sooner than the in phase front left (blue) paw, as compared with previous cycles. The mouse is using a trotting gait here, diagonal pairs of limbs are in phase. (c) Example data for non-invasive quantification of ankle torque production as a function of direct LG muscle activation with 10 mA. (For interpretation of the references to color in this figure legend, the reader is referred to the web version of this article.)

monitored every other day and Neosporin ointment was applied around the incision. The headmounts (n = 8) remained in place for an average of 25 days (SD = 4.75), ranging from 19 to 33 days before falling off the head.

Later, we built seven headmounts with shorted connections between the two magnets on the animal side using 8 cm stainless steel wires and implanted on the head of seven mice to check for the resistivity and reliability of the device. To measure the resistance of the headmount apparatus, the implanted headmount was connected to a voltmeter through the headmount coupler. The measurements were taken once a

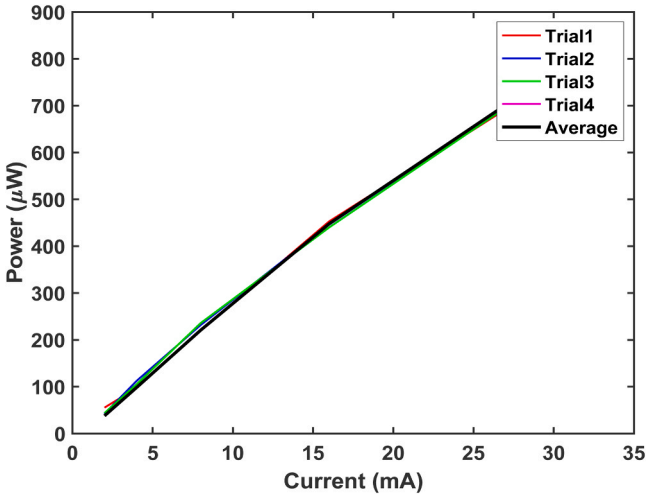

Fig. 7. Validating the headmount for optical stimulation. Optical power produced by the optical cuff coupled with the headmount system using different currents. Optical power measurements demonstrating an approximately linear response to increased current (Thorlabs PM100D, LED cuff to detector distance 15 mm, total current to LED array 12 mA). Note that this measurement was designed to test linearity at low light intensity, which may be important for nerve recruitment studies, and was not a test of maximum light intensity. To estimate the maximal optical power incident on the nerve, the same detector was placed at close as possible to the cuff (~3 mm), and an optical power measurement of 21.3 mW at a current of 59.2 mA through the entire 18 LED element array, or 9.86 mA per LED (PICOLED part #SMLP13BC8TT86; maximum current 10 mA; array consisting of 6 linear arrays of 3 LEDs in series; e.g., 6 "strings" of 3 LEDs in series were placed in parallel, thus current per LED is 59.2 mA/6 = 9.86 mA).

week after each surgery. The DC resistance of the headmounts (n = 7) was averaged 12.95 ohms (SD = 0.83), ranging from 12.22 ohm to 14.75 ohm across both magnets. The average change of the resistance in each headmount through the weeks of measurements was 0.58 ohms (SD = 1.13).

Because microsecond time-scale changes in resistance at the magnet interface could cause rapid changes in voltage and thus stimulation current, when stimulation is occurring and when a voltage clamped current stimulator is in use, we sought to determine whether there are microsecond changes in resistance at the headstage coupling. To provide a controlled test that is a reasonable simulacrum of headstage movement whilst attached to a rodent, we taped a shorted headstage to a HexBug Nano toy robot (https://www.hexbug.com/nano), that vibrates and moves on a surface in a rough approximation to a rodent – in fact, the continuous, relatively high amplitude vibrations of the HexBug are likely significantly larger than for a mouse. To determine whether there are transient changes in resistance, we used a 9 V battery, voltage divider, and a National Instruments USB-6212 device to record 20 min of Analog Voltage at 10 kHz, whilst the HexBug was moving, and examined the analog voltage recordings for noise level (Fig. 5a). The circuit including the Cooner AS633 stainless steel lead wires through the shorted headstage had a resistance of ~150 Ohms. The voltage divider was made of resistances of 44k Ohm on the "top" resistor and 22k Ohm on the "bottom" resistor, and the headstage was placed in series with the divider after the 22k Ohm resistor. Measurement of voltage was made between the 44k Ohm and 22k Ohm resistors, and thus about 2.9 V was the DC voltage. The hex bug was picked up and switched on, and placed back inside a small cardboard box to vibrate and roam freely for 20 min (Fig. 5b). No large upward jumps in voltage, corresponding to a disconnect, were observed during the 20 min (Fig. 5c), where the voltage remained stable with mean voltage 2.97 V and standard error 0.8 mV. A sanity check that the voltage went to supply voltage upon disconnection of a headstage magnet was performed after 20 min of

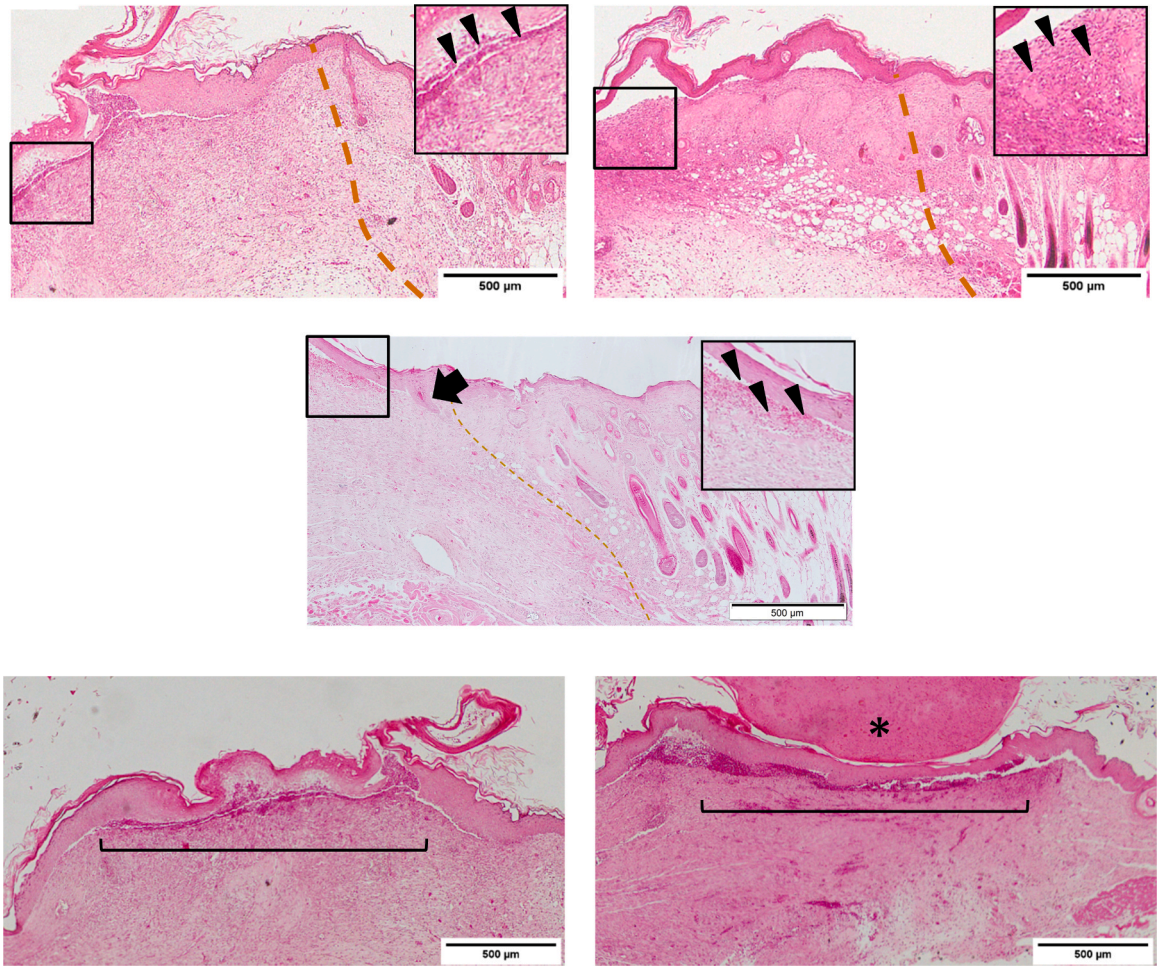

Fig. 8. Headmount biocompatibility after implantation. (a) Micrographs of hematoxylin and eosin stained tissue. Wounded site and healthy skin are to the left and right of the perforated line respectively. Note the abundance of inflammatory cells recruited to the newly forming dermis (pointed to using arrow heads in high-magnification view). Restoration of a hair follicle is also observed in the healing site indicated by the arrow. (b) Representative hematology and eosin staining of skin. The black brackets indicates the implant site of headmount. No signs of toxicity or inflamation was detected at the implantation site. Asterisk indicates serocellular crust.

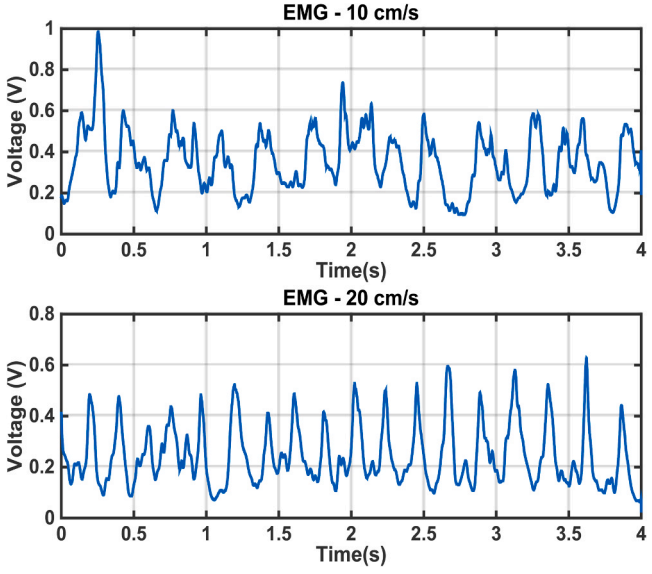

Fig. 9. Validating the headmount for EMG. The LG muscle activity of the mouse while running on the treadmill with a belt speed of 10 cm/s, and 20 cm/s.

recording (Fig. 5d).

3.2. Electrical nerve stimulation

Here we present data on the kinematic response of a mouse to a sudden electrical nerve stimulation. For this purpose, we implanted cuff electrodes (§ 2.4.1) around the sciatic nerve coupled with the headmount implanted on the skull of the mouse. After the muscle physiology characterization using the Aurora system, 0.1–1 mA was found to be a suitable range of current for the nerve stimulation. We later applied different currents starting from 0.1 mA to the sciatic nerve of the mouse while the animal was trotting on the treadmill and increased the current by 0.1 mA for each trial. Fig. 6a indicates the fore/aft paw positions of the mouse for ~1 s before, and ~0.5 s after the electrical nerve stimulation with 0.4 mA.

3.3. Electrical muscle stimulation and EMG

After implanting the electrodes in the LG muscle of the mice, we validated muscle stimulation by measuring force development as a function of direct electrical stimulation of muscle. We stimulated the muscle using different currents ranging from 1 mA to 20 mA and the torque produced by the muscle was recorded. Stimulus pulse trains were 30 ms in duration at 100 Hz frequency, with a duty cycle of 0.1. Fig. 6c

illustrates example data for an ankle torque produced by a 10 mA stimulation current in a mouse. We later used the same group of mice and stimulated the LG muscle while the animal was trotting on the treadmill to perturb their gait. The adequate amount of current for the gait perturbation of each mouse was indicated during their muscle physiology characterization experiment. Fig. 6b shows the paw position of a mouse during a 3.5 mA muscle stimulation.

A brief summary of how the headmount functions when recording muscle activity is given in the Appendix.

3.4. Optical nerve stimulation

We connected the optical cuff to an LED driver (BuckPuck 3021-D-E-1000) powered by a 9 V battery through the headmount and the headmount coupler to measure the emitted optical power produced by holding the flattened cuff ~15 mm away from a power meter (Thorlabs PM100D). Fig. 7 illustrates the output optical power in response to increased current.

3.5. Biocompatibility

We assessed the quality of healing skin at the site of headmount implantation. Hemotoxylin and eosin staining of transvers sections of skin tissue showed a natural-like healing of the skin evidenced by a very well organized and stratified epithelial layer. In Fig. 8 panel a, the healthy/healing margin for one of the mice is marked by a perforated line. On the left of the border is the healing skin with the newly formed epidermis with a hair follicle (arrow) restored which clearly shows a normal healing process in progress. The granulated tissue underneath the epidermis however, contains inflammatory/ immune cells (arrow heads) recruited to the wound site showing a moderate ongoing inflammatory response in action. This immune cell recruitment is triggered by the effective local damage imposed to the skin for headmount implantation and is an essential phenomenon for initiation and progression of the healing process.

The headmounts appeared to be well tolerated by the mice with no signs of adverse reaction such as infection or tissue necrosis. The newly formed skin furthermore showed to be quite functional having engulfed the headmount (Fig. 8 panel b) with no signs of toxicity or bioincompatibility. Perseverance of the immune cells (dark purple) at the site of the implant (See the brackets in Fig. 8 panel b) demonstrates an ongoing inflammatory response. We surmise that this persistent inflammatory response is a result of the presence of the foreign body i.e. the headmount. The local accumulation of inflammatory cells at the implant site along with its' marked decrease in distances farther away from the implant is one of the in vivo manifestations of a foreign body reaction (Abee et al., 2012), which may persist as long as the foreign body exists (Atala et al., 2018).

4. Discussion

Here we have introduced a lightweight 'snap-in' magnetically coupled nerve and muscle recording and stimulation headmount. The magnetic connection allows the animal to be 'snapped' into the instrumentation setup (stimulator or recorder) with extremely little prep and results in near zero insertion force, causing less stress on animal and researcher. Additionally, the lightweight neural device is very small and uses strong neodymium magnets to enable a reliable connection without excess weight. Furthermore, it avoids using screws or dental acrylic to directly attach to the bone, thus reducing the chance of damage or perforation of the skull during surgery. The conductivity of the device is stable, as our resistivity measurements showed a reliably low resistance across headmounts and over time.

The headmount is made of PDMS, which isolates the wires from the tissues and the body liquid, protecting the animal from electrical shock and preventing electrical short circuit. PDMS has long been known for its biocompatibility, flexibility and durability and has been widely used for manufacturing cosmetic fillers, contact lenses and implantable medical devices in human studies. Although long term (up to 2 months) subcutaneous implantation of PDMS has shown fibrotic reactions progressing over the course of studies, no major inflammatory reaction has been reported (Timnak et al., 2018). A normal inflammatory phase is however necessary to initiate wound healing process and its' progression. In a normal wound healing process, immediately after hemostasis, the second phase of wound healing, i.e. inflammation stage, initiates deploying and recruiting polymorphoneuclear and mononuclear cells to the site of injury (Timnak et al., 2018). Chemotactic stimuli sent out by the inflammatory mediators trigger wound debridement, granulation tissue formation, and re-epithelialization (Broughton et al., 2006; Andrade et al., 2011). Fig. 8 panel b indicates the restoration of the epithelium and the successful resolution of inflammation and progression of the healing process throughout with no cytotoxicity effect. Formation of serocellular crust or commonly known as scab, pictured in panel b of Fig. 8 with an asterisk is believed to induce hemostasis, reduce inflammation, and improve the healing process (Lin et al., 2020; Hissong et al., 2017) and does not defeat biocompatibility of the implant. Furthermore, the skin appears to be quite functional as it firmly envelopes the headmount (Fig. 2g).

As the result, the device has demonstrated itself to be robust, enhancing animal wellbeing during and between experiments. Our preliminary data also indicates that device can successfully be used for electrical nerve and muscle stimulation, electromyography, and optical stimulation purposes.

Further work will seek to add to the number of connectors that can be passed through. The two magnets used here also served as signal passthroughs. Future designs could use the magnets for alignment and attachment, but use a higher density method for passing through signals, such as a ball grid array, allowing for more connections. Recording of several channels of EMG would be desirable, as would mixed interfaces for simultaneously recording and stimulating at multiple locations.

CRediT authorship contribution statement

Annie Vahedipour: Conceptualization, Data curation, Investigation, Methodology, Project administration, Resources, Validation, Visualization, Writing – original draft. **Mathew Short:** Investigation, Validation, Visualization, Writing – review & editing. **Azadeh Timnak:** Data curation, Investigation, Methodology, Validation, Visualization, Writing – review & editing. **Omid Haji Maghsoudi:** Investigation, Software, Visualization, Writing – review & editing. **Thomas Hallowell:** Investigation, Validation. **Jonathan Gerstenhaber:** Methodology, Validation, Resources. **Ornella Cappellari:** Methodology, Resources. **Michel Lemay**: Conceptualization, Methodology, Resources, Supervision. **Andrew Spence:** Conceptualization, Funding acquisition, Methodology, Project administration, Resources, Software, Supervision, Visualization, Writing – review & editing.

Acknowledgements

This material is based upon work supported by, or in part by, the U. S. Army Research Laboratory and the U.S. Army Research Office (Grant no: W911NF1410141), a Shriners Hospitals for Children Senior Research Grant (#85115), and a Craig H. Neilsen Foundation Senior Research Grant (#546798), to A.J.S.

Conflict of interest

The authors declare no competing financial interests.

Appendix

The headmount can also be used when recording muscle activity

(electromyography; EMG). A mouse with electrodes implanted in the lateral gastrocnemius (LG) muscle was placed on the treadmill and EMG signal from this muscle was recorded through the headmount (Fig. 9). While in this instance the recording looks unipolar and does not look like a typical EMG, the oscillations in the recordings were of the same frequency as the animal strides as measured in high-speed video, for two trials with different stride frequencies. We believe the noisy signal was due to one intramuscular EMG lead having movement artifact, which will be corrected in future work. This experiment provides a simple proof of concept that EMG signals can be passed through the headmount.

References

Abee, C.R., Mansfield, K., Tardif, S.D., Morris, T. (Eds.), 2012. Nonhuman primates in biomedical research: biology and management, 1. Academic Press.

Akay, T., Tourtellotte, W.G., Arber, S., Jessell, T.M., 2014. Degradation of mouse locomotor pattern in the absence of proprioceptive sensory feedback. Proc. Natl. Acad. Sci. USA 111 (47), 16877–16882.

Andrade, T.A.M., Iyer, A., Das, P.K., Foss, N.T., Garcia, S.B., Coutinho-Netto, J., Frade, M. A.C., 2011. The inflammatory stimulus of a natural latex biomembrane improves healing in mice. Braz. J. Med. Biol. Res. 44 (10), 1036–1047.

Arenkiel, B.R., Peca, J., Davison, I.G., Feliciano, C., Deisseroth, K., Augustine, G.J., Feng, G., 2007. In vivo light-induced activation of neural circuitry in transgenic mice expressing channelrhodopsin-2. Neuron 54 (2), 205–218.

Atala, A., Lanza, R., Mikos, T., Nerem, R., 2018. Principles of Regenerative Medicine (Eds.). Academic Press.

Bellardita, C., Kiehn, O., 2015. Phenotypic characterization of speed-associated gait changes in mice reveals modular organization of locomotor networks. Curr. Biol. 25 (11), 1426–1436.

Broughton, I.I., Janis, J.E., Attinger, C.E., 2006. Wound healing: an overview. Plast. Reconstr. Surg. 117 (7S), 1e–S–32e-S.

Caggiano, V., Sur, M., Bizzi, E., 2014. Rostro-caudal inhibition of hindlimb movements in the spinal cord of mice. PLoS One 9 (6), e100865.

Costa, R.M., Federov, N.B., Kogan, J.H., Murphy, G.G., Stern, J., Ohno, M., Silva, A.J., 2002. Mechanism for the learning deficits in a mouse model of neurofibromatosis type 1. Nature 415 (6871), 526–530.

Deisseroth, K., 2011. Optogenetics. Nat. Methods 8 (1), 26–29.

Dobkin, B.H., Harkema, S., Requejo, P., Edgerton, V.R., 1995. Modulation of locomotor-like EMG activity in subjects with complete and incomplete spinal cord injury. J. Neurol. Rehabil. 9 (4), 183–190.

Dutta, Sulagna, Sengupta, Pallav, 2016. Men and mice: relating their ages. Life Sci. 152, 244–248.

Harris-Warrick, R.M., 2011. Neuromodulation and flexibility in central pattern generator networks. Curr. Opin. Neurobiol. 21 (5), 685–692.

Hashimoto, Mitsuhiro, Hata, Akihiro, Miyata, Takaki, Hirase, Hajime, 2014. Programmable wireless light-emitting diode stimulator for chronic stimulation of optogenetic molecules in freely moving mice. Neurophotonics 1 (1), 011002.

Haugland, M. A flexible method for fabrication of nerve cuff electrodes. In: Proceedings of the Eighteenth Annual International Conference of the IEEE, Bridging Disciplines for Biomedicine, Engineering in Medicine and Biology Society, IEEE, 1, (1996, November) 359–360).

Hissong, J.B., Myntti, M.F., Medina, J.G., U.S. Patent No. 9,700,648, U.S. Patent and Trademark Office, Washington, DC, (2017).

Jeong, J.W., McCall, J.G., Shin, G., Zhang, Y., Al-Hasani, R., Kim, M., Li, S., Sim, J.Y., Jang, K.I., Shi, Y., Hong, D.Y., Liu, Y., Schmitz, G.P., Xia, L., He, Z., Gamble, P., Ray, W.Z., Huang, Y., Bruchas, M.R., Rogers, J.A., 2015. Wireless optofluidic systems for programmable in vivo pharmacology and optogenetics. Cell 162 (3), 662–674.

Kadekaro, M., Crane, A.M., Sokoloff, L., 1985. Differential effects of electrical stimulation of sciatic nerve on metabolic activity in spinal cord and dorsal root ganglion in the rat. Proc. Natl. Acad. Sci. USA 82 (17), 6010–6013.

Kitanishi, Takuma, Umaba, Ryoko, Mizuseki, Kenji, 2021. Robust information routing by dorsal subiculum neurons. Sci. Adv. 7 (11), eabf1913.

Kravitz, A.V., Freeze, B.S., Parker, P.R., Kay, K., Thwin, M.T., Deisseroth, K., Kreitzer, A. C., 2010. Regulation of parkinsonian motor behaviours by optogenetic control of basal ganglia circuitry. Nature 466 (7306), 622–626.

Lathe, R. Mice, 1996. gene targeting and behaviour: more than just genetic background. Trends Neurosci. 19 (5), 183–186.

Lee, Byunghun, Koripalli, Mukhesh K., Jia, Yaoyao, Acosta, Joshua, Sendi, M.S.E., Choi, Yoonsu, Ghovanloo, Maysam, 2018a. An implantable peripheral nerve recording and stimulation system for experiments on freely moving animal subjects. Sci. Rep. 8 (1), 1–12.

Lee, Byunghun, Koripalli, Mukhesh K., Jia, Yaoyao, Acosta, Joshua, Sendi, M.S.E., Choi, Yoonsu, Ghovanloo, Maysam, 2018b. An implantable peripheral nerve recording and stimulation system for experiments on freely moving animal subjects. Sci. Rep. 8 (1), 1–12.

Lin, J.Y., Luo, S.H., Chen, S.H., Yang, L.T., Xiao, Y., Huang, Z.H., Wang, Z.Y., 2020. Efficient synthesis, characterization, and application of biobased scab-bionic hemostatic polymers. Polym. J. 52, 615–627.

Llewelyn, J., Phillips, B.L., Alford, R.A., Schwarzkopf, L., Shine, R., 2010. Locomotor performance in an invasive species: cane toads from the invasion front have greater endurance, but not speed, compared to conspecifics from a long- colonised area. Oecologia 162 (2), 343–348.

Maghsoudi, O.H., Vahedipour, A., Spence, A., 2019. A novel method for robust markerless tracking of rodent paws in 3D. EURASIP J. Image Video Process. 2019 (1), 79.

Marrosu, F., Santoni, F., Fà, M., Puligheddu, M., Barberini, L., Genugu, F., Mereu, G., 2006. Beta and gamma range EEG power-spectrum correlation with spiking discharges in DBA/2J mice absence model: role of GABAB receptors. Epilepsia 47 (3), 489–494.

Montgomery, K.L., Yeh, A.J., Ho, J.S., Tsao, V., Mohan Iyer, S., Grosenick, L., Ferenczi, E. A., Tanabe, Y., Deisseroth, K., Delp, S.L., Poon, A.S., 2015. Wirelessly powered, fully internal optogenetics for brain, spinal and peripheral circuits in mice. Nat. Methods 12 (10), 969–974.

Moreno-Duarte, I., Morse, L.R., Alam, M., Bikson, M., Zafonte, R., Fregni, F., 2014. Targeted therapies using electrical and magnetic neural stimulation for the treatment of chronic pain in spinal cord injury. NeuroImage 85, 1003–1013.

Ortiz-Catalan, M., Håkansson, B., Brånemark, R., 2014. Real-time and simultaneous control of artificial limbs based on pattern recognition algorithms. IEEE Trans. Neural Syst. Rehabil. Eng. 22 (4), 756–764.

Park, Sohee, Liu, Cai-yue, Ward, Patricia J., Jaiswal, Poonam B., English, Arthur W., 2019. Effects of repeated 20-hz electrical stimulation on functional recovery following peripheral nerve injury. Neurorehabilit. Neural Repair 33 (9), 775–784.

Riban, V., Bouilleret, V., Pham-Le, B.T., Fritschy, J.M., Marescaux, C., Depaulis, A., 2002. Evolution of hippocampal epileptic activity during the development of hippocampal sclerosis in a mouse model of temporal lobe epilepsy. Neuroscience 112 (1), 101–111.

Song, K.I., Park, S.E., Lee, S., Kim, H., Lee, S.H., Youn, I., 2018. Compact optical nerve cuff electrode for simultaneous neural activity monitoring and optogenetic stimulation of peripheral nerves. Sci. Rep. 8, 15630.

Spence, A.J., Nicholson-Thomas, G., Lampe, R., 2013. Closing the loop in legged neuromechanics: an open-source computer vision controlled treadmill. J. Neurosci. Methods 215 (2), 164–169.

Talpalar, A.E., Kiehn, O., 2010. Glutamatergic mechanisms for speed control and network operation in the rodent locomotor CPG. Front. Neural Circuits 4, 19.

Timnak, A., Gerstenhaber, J.A., Dong, K., Lelkes, P.I., 2018. Gradient porous fibrous scaffolds: a novel approach to improving cell penetration in electrospun scaffolds. Biomed. Mater. 13 (6), 065010.

Vahedipour, A., Maghsoudi, O.H., Wilshin, S., Shamble, P., Robertson, B., Spence, A., 2018. Uncovering the structure of the mouse gait controller: mice respond to substrate perturbations with adaptations in gait on a continuum between trot and bound. J. Biomech. 78, 77–86.

Wang, J., Kannape, O.A., Herr, H.M., Proportional EMG control of ankle plantar flexion in a powered transtibial prosthesis. In: Proceedings of the IEEE International Conference, Rehabilitation Robotics (ICORR), IEEE, (2013, June), 1–5.

Wu, C., Wais, M., Sheppy, E., del Campo, M., Zhang, L., 2008. A glue-based, screw- free method for implantation of intra-cranial electrodes in young mice. J. Neurosci. Methods 171 (1), 126–131.

Wu, C., Wais, M., Zahid, T., Wan, Q., Zhang, L., 2009. An improved screw-free method for electrode implantation and intracranial electroencephalographic rcordings in mice. Behav. Res. Methods 41 (3), 736–741.

Zhang, Y., Mickle, A.D., Gutruf, P., McIlvried, L.A., Guo, H., Wu, Y., Golden, J.P., Xue, Y., Grajales-Reyes, J.G., Wang, X., Krishnan, S., Xie, Y., Peng, D., Su, C.J., Zhang, F., Reeder, J.T., Vogt, S.K., Huang, Y., Rogers, J.A., Gereau, R.W., 2019. Battery-free, fully implantable optofluidic cuff system for wireless optogenetic and pharmacological neuromodulation of peripheral nerves. Sci. Adv. 5 (7), 5296.